Journal of the European Ceramic Society 22 (2002) 2047–2059

www.elsevier.com/locate/jeurceramsoc

Structural and mechanical properties of a high-performance BN fibre

S. Bernard*, F. Chassagneux, M.-P. Berthet, H. Vincent, J. Bouix

Laboratoire des Multimatériaux et Interfaces, UMR CNRS 5615, B,t. Berthollet, Université Claude Bernard, Lyon1, 43, Bd du 11 Novembre 1918, 69622 Villeurbanne Cedex, France

Received 12 July 2001; received in revised form 16 November 2001; accepted 8 December 2001

Abstract

The relationship between the structure, microtexture and mechanical properties of a high-performance polyborazine-based BN fibre has been studied in detail. Techniques such as Raman and IRTF spectroscopies, X-ray diffraction, scanning and transmission electron microscopies and microtraction tests were used. It has been shown that the longitudinal mechanical properties of the fibre directly depend on the microtextural and structural properties. In particular, the Young's modulus in the fibre-axis ($E=440$ GPa) is directly controlled by the fibre structure: the fibre presents a high degree of alignment of the (002) planes compared with the fibre axis ($\tau=0.90$) and the high value of the elastic modulus in the fibre-axis is attributed to the strong covalent bonds in the basal planes. On the other hand, the ultimate tensile strength ($\sigma^R=2000$ MPa) and the low density ($d=1.85$ g cm^{-3}) of the fibre are limited by the external defects and the porosity in the volume of the fibre. © 2002 Published by Elsevier Science Ltd.

Keywords: BN fibre; Defects; Elastic modulus; Fibres; Strength; Structure

1. Introduction

The development of the ceramic-matrix composites (CMCs) and metal-matrix composites (MMCs) represents a technological interest. It depends on a reinforcement with high-performance ceramic fibres and on the fibre-matrix combination. The high longitudinal mechanical properties and low densities of fibres as carbon or silicon carbide when combined with a ceramic and metal-matrix produce a class of materials possessing specific properties as lightness, stiffness and high failure strength. Pitch and PAN-based carbon fibres are by far the predominant high strength and high elastic modulus reinforcements used in the fabrication of high-performance CMCs and MMCs. The high longitudinal mechanical properties of the carbon fibres are a direct result of the anisotropy found in the graphite crystal.

Owing to a low density ($d=2.26$ g cm^{-3}), a chemical inertia with molten metals and a similar anisotropic structure to graphite, the use of hexagonal boron nitride (*h*-BN) fibres appears attractive for CMC and MMC reinforcements. The first BN fibres were investigated by Economy et al.[1]. The process consisted to a chemical conversion of boric-oxide (B_2O_3) fibres into BN fibres by gas-solid reactions in ammonia atmosphere then, the fibres underwent a high processing temperature. They presented a good average tensile strength ($\sigma^R=1000$ MPa) and the process was fast but a meticulous control of the nitridation was required. The interest for polymeric precursors has then increased for their shaping and relationships with the ceramic materials. The pyrolysis technique makes it much easier to obtain very long, fine diameter and flexible BN fibres compared with the nitridation process. It is a matter of a preceramic method which consists of the molecular precursor synthesis and its polymerization into a polymeric precursor. The polymer is melt-spun and heated to high temperature. Kimura et al[2], Paciorek and Kratzer,[3] Narula et al.,[4] and Wideman et al.,[5] have prepared fibres by this method from many types of polyborazine. In our laboratory, we have recently developped BN fibres from polyborazine [6,7] as preceramic polymer and, in the present paper, we evaluate the different chemical and physical properties of a poly[2,4,6-tri(methylamino)borazine]-based BN fibre with high mechanical properties.

* Corresponding author.
E-mail address: sbernard@univ-lyon1.fr (S. Bernard).

0955-2219/02/$ - see front matter © 2002 Published by Elsevier Science Ltd.
PII: S0955-2219(01)00524-6

2. Experimental procedure

2.1. Characterization techniques

The qualitative analysis of the BN fibre is performed by infrarouge spectroscopy between 400 and 4000 cm^{-1}. Transmission infrared spectra is obtained using a Fourier Transform (FT-IR) spectrometer (Nicolet, Magna-IR, Spectrometer 550). The fibre is grinded then mixed with KBr for the FT-IR measurements. This characterization method is completed by Raman spectroscopy microanalysis between 1200 and 1700 cm^{-1} (Olympus BX60 Hololab series 5000, lateral resolution: 1 μm). Analyses are carried out by pointing the laser source ($\lambda = 784.698$ nm, 100 mW) directly on the surface of one fibre.

Tensile tests are performed at room temperature on single fibres with several gauge lengths (10, 20 and 30 mm). Individual filaments are carefully removed from a part of yarn and their diameters are measured by interferometry. The two ends of each filament are glued with cyanocrylate on a cardboard for handling and testing. A mounting system including two grips, a displacement transducer and a load cell (5 N) is set on a standard tensile tester (Adamel Lhomargy DY 22). Tensile tests are then achieved with an crosshead speed of 0.1 mm/min. The fibre is characterized from 50 measures according to the Weibull statistics.[8]

The pyrolysis of the fibre is studied by thermogravimetric analysis (TGA92–16.18 from Setaram) under an ammonia/nitrogen mixture (1 l h^{-1}/1 l h^{-1}) then nitrogen atmosphere (1 l h^{-1}). Experiments are performed on 70–80 mg samples heated at a rate of 0.8 °C min^{-1} up to 1500 °C.

Scanning electron microscopy (SEM) is used to observe the surface morphology and the cross-section of the fibre (Hitachi S800). In the sample preparation, BN filaments are glued on a aluminum support and metallized.

The X-ray diffraction (XRD) patterns in the 2θ ranging from 15 to 85° using a Phillips apparatus and Cu$K_{\alpha 1}$ radiation are recorded from a tow. The specimens are placed in the position so that the fibre-axis is perpendicular to incidence plane. Comparatively, the XRD patterns are recorded from the same fibre after crushing. X-ray diffraction data have been used to obtain information about the interlayer spacing d_{002}, the average stack height $\overline{L_c}$ and the average length $\overline{L_a}$ (or length of straight basal planes in the crystallites) and the preferred orientation of hexagonal layers (002 planes) parallel to the fibre-axis. The dimension d_{002} is calculed from Bragg's law using the diffraction angle of the (002) peak. The average stack height $\overline{L_c}$ is calculated from the Scherrer relation:

$$\overline{L_c} = 0.9\ \lambda/(B^2 - B'^2)^{1/2}\cos\theta$$

where λ is the Cu$K_{\alpha 1}$ wavelength ($\lambda = 0.1540$ nm), θ the Bragg angle of the (002) diffraction peak, B the full width at half maximum intensity (FWHM) of the peak and B' the instrumental contribution.

The average length $\overline{L_a}$ is calculated from the FWHM of the (10) diffraction peak on the crushed fibre according to the Scherrer relation:

$$\overline{L_a} = 1.84\lambda/(B^2 - B'^2)^{1/2}\cos\theta$$

The preferred orientation of hexagonal layers compared with the fibre-axis is obtained by the analysis of the (002) and (10) peaks intensity ratio in the fibre and crushed fibre patterns. The crushed fibre XRD indicates a random crystallite orientation in the fibre volume and, consequently, the intensities of (002) and (10) diffraction peaks are similar to those recorded from polycrystalline hexagonal BN materials. On the other hand, the fibre XRD pattern reveals a better alignment of the crystallites in the fibre-axis: the intensity of (002) peak is increased and the intensity of (10) diffraction peak is decreased. It means that the (002) planes are in the Bragg position while the (10) planes are perpendicular to the (002) planes. The degree of crystallites orientation compared with the fibre-axis τ is calculated by the relation:

$$\tau = (R_{\text{fibre}} - R_{\text{crushed fibre}})/R_{\text{fibre}}$$

where R is the ratio between (002) and (10) peak intensities in the corresponding diffractogramm: $R = I_{(002)}/I_{(10)}$.

The higher the ratio R in fibre diffractogram, the higher the axial preferred crystallite orientation.

The microstructure of the fibre is studied by transmission electron microscopy (TEM) using a Topcon 002B microscope. The samples are embedded in a resin and cut into thin foils with an ultramicrotome. Foils are then set on copper microgrids. The foils are prepared to observe the fibre as well cross-section as longitudinal section. The textural parameters such as L_c, $L_{a//}$ and $L_{a\perp}$ are calculated. The TEM analyses are performed in the bright-field (BF), (002) dark-field ((002) DF), lattice-fringes (002) and selected area diffraction (SAD) modes for both longitudinal and transverse sections. The degree of crystallite orientation τ compared with the fibre-axis is determined by measuring the spread of electron diffraction along the (002) arc: the smaller the spread of the arc, the higher the degree of crystallite alignment in the fibre-axis. The degree of orientation τ ?is calculated by the relation:

$$\tau = (180 - \zeta)/180$$

where ζ is the misorientation angle of the (002) planes.

The shape, the dimensions (L_c, L_a) and the crystallite arrangement have been determined by combining the

various modes of imaging and the two directions of sectioning.

2.2. BN fibres process

Standard inert atmosphere techniques are used in the syntheses, manipulation and melt-spinning.

2.2.1. Polymeric precursor synthesis

Poly[2,4,6-tri(methylamino)borazine] (PolyMAB) is prepared by thermal condensation in bulk of 2,4,6-tri(-methylamino)borazine (MAB)[6,9] under a flow of argon. The characteristics of the polymer used in this study are presented in Table 1 and depend on thermal cycles.

2.2.2. Preparation of the polyMAB's raw fibres and continuous BN fibres

The polymer placed in a little vertical furnace is molten under nitrogen atmosphere at a temperature at which it exhibits a suitable viscosity. A piston is pushed down at a constant rate. The polymer is extruded through a spinneret and it is stretched by means of a spool which turns at a constant rate to produce continuous polymeric fibres. The continuous raw fibres on the spool are become infusible fibres by means of heat treatment in a flow of ammonia gas at low and intermediate temperature. After that, a high temperature treatment in a nitrogen flow is realized to crystallize the fibres on the spool. The fibres are maintened at this temperature for one hour and cooled down to room temperature. The Kimura's process was different. The fibre surface was slightly hydrolyzed and became infusible in the spinning process while in this paper the raw fibre is not hydrolyzed but it become infusible with the use of NH_3 atmosphere. Moreover, the Kimura's pyrolysis process with spool was not used. Indeed, several pieces of the raw filament were placed on an alumina boat and transferred to an electric tube furnace up to 1800 °C.

3. Results

3.1. FT–IR and Raman analysis

The layers of *h*-BN are stacked in a hexagonal crystal structure corresponding to the space group $P6_3/mmc$ (D^4_{6h}). The zone-center optic phonons can be decomposed into the following irreductible representation:[10]

$$\Gamma = A_{2u} + 2B_{1g} + E_{1u} + 2E_{2g}$$

The E symmetry modes exhibit "in-plane" atoms displacements while the A and B symmetry modes have "out of plane" displacements. The A_{2u} and E_{1u} modes are IR active, the B_{1g} modes are optically inactive and only the E_{2g} modes are expected to Raman active as fundamentals.

FT–IR between 400 and 4000 cm^{-1} and the Raman in the ranging from 1200 to 1700 cm^{-1} spectra obtained from the BN fibre are shown in Fig. 1. The infrared spectra shows a strong and broad absorption band centered at 1367 cm^{-1} and a sharp weak band at 805 cm^{-1}. The wavelength IR absorption bands are characteristic of specific types of chemical bonds B–N in *h*-BN.[11] The bands are assigned in plane ring vibration at 1367 cm^{-1} (E_{1u} mode) and out of the plane ring vibration at 805 cm^{-1} (A_{2u} mode) respectively.

The single Raman active band at 1367 cm^{-1} corresponds to the typical vibration frequency observed in *h*-BN materials.[10] It is due to the E_{2g} symmetric vibration mode in *h*-BN (B–N in plane atomic displacements).

Table 1
Chemical characteristics of poly[2,4,6-tri(methylamino)borazine]

Δm (wt.%)[a]	T_g (°C)	C (wt.%)	H (wt.%)	N (wt.%)	B (wt.%)
24	84	19.4	7.6	47	26

[a] Δm, Weight loss due to the thermal polycondensation of MAB.

3.2. Mechanical properties

Individual fibres (about 50 specimens) are carefully pulled out from the same zone of the tow and submitted to tensile tests. At room temperature, the fibre exhibits linear behaviour in tension with brittle failure. The ultimate tensile strengths with 10 mm gauge lengths as a function of the survival probability P_s are shown in a Weibull plot in Fig. 2. The strength distribution plotted in the Weibull diagram is not strictly linear and the Weibull parameter is low ($m = 2.3$). Although the strength values of the fibres are distributed in a large range from 800 to 2800 MPa, the majority of filaments exhibits tensile strengths above 1800 MPa and the strongest ones exceeded 2300 MPa while the highest tensile strength obtained by Kimura et al. [2] at the same final pyrolysis temperature and from a polyMAB precursor were 980 MPa. The strength calculated for a failure probability P_r ($P_r = 1 - P_s$) of 63% is $\sigma^R = 2000$ MPa. The highest failure strength values are generally obtained for filaments with a small diameter as is shown in Fig. 3. The stress-elongation straight line drawn from the rupture tests (Fig. 4) proves that the fibre has an elastic behaviour. The Young's modulus is determined by the slope of this curve (440 GPa) and the values are distributed in a much narrower range compared to the tensile strength values. These values are higher than the tensile modulus obtained by Kimura et al.[2] (78 GPa). Fig. 5 and Table 2 show the dependence on mechanical properties of the fibre upon the gauge length. It can be seen that the measured tensile strength for a failure probability P_r of 63% increases as the gauge length decreases whereas the Young's modulus remains

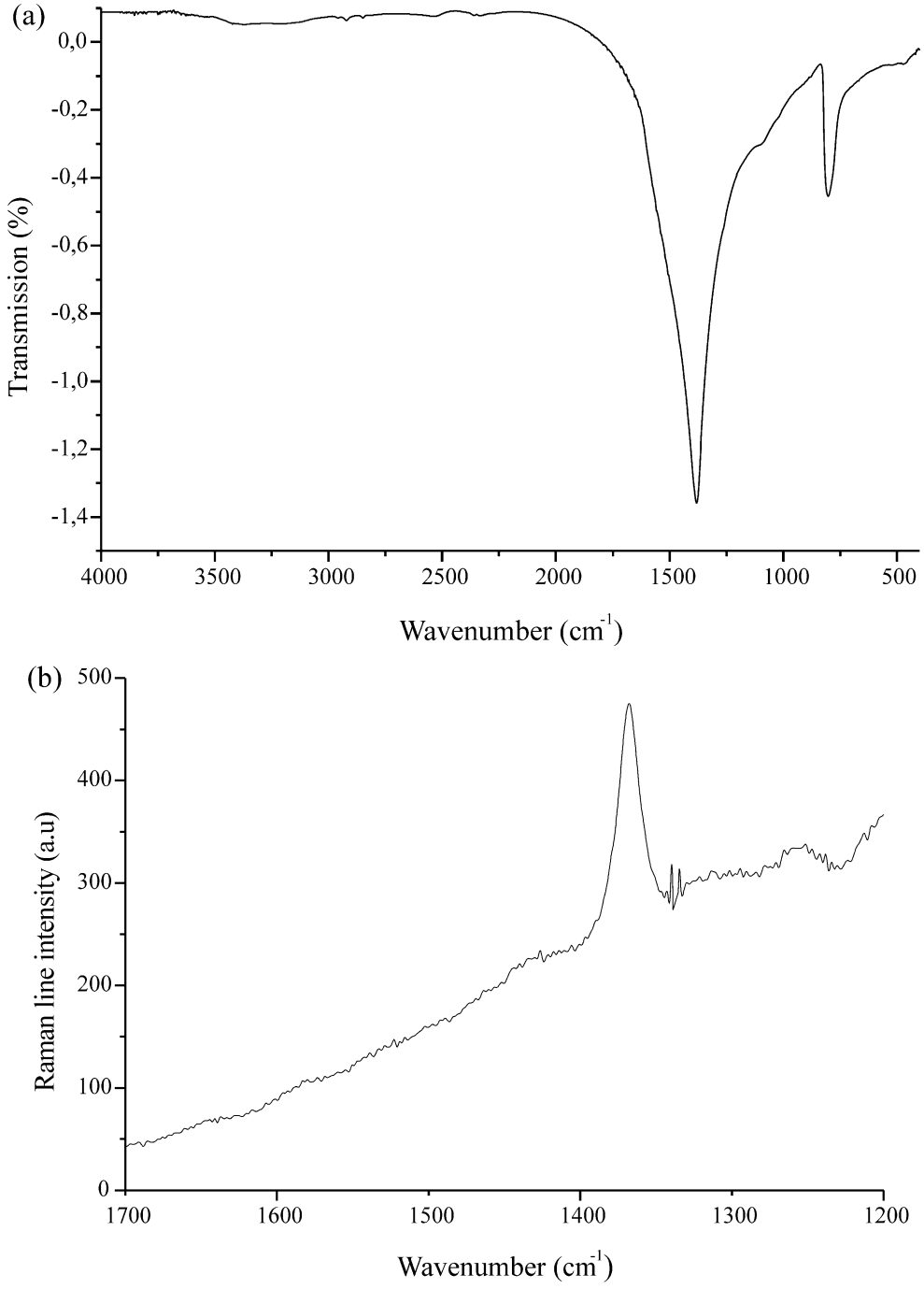

Fig. 1. (a) FT–IR and (b) Raman spectra of BN fibres pyrolyzed at 1800 °C.

Table 2
Mechanical properties as a function of gauge length

Diameter ϕ (μm)	Tensile strength σ^R (MPa)	Young's modulus (GPa)	Weibull modulus m	Gauge length (mm)
10.7	2000	440	2.3	10
10.4	1580	450	2.2	20
10.6	1190	435	2.2	30

unchanged. The variation of tensile strength with gauge length shows an approximately linear behaviour. The strong dependence on the tensile strength upon gauge length and volume of the fibre is due to the presence of defects as voids and cracks. In this high-performance fibre, the defects were not present in the raw fibre after the melt-spinning and stretching processes. The internal defects as pores rather appear when the gaseous products are evolved during the pyrolysis of the polymeric

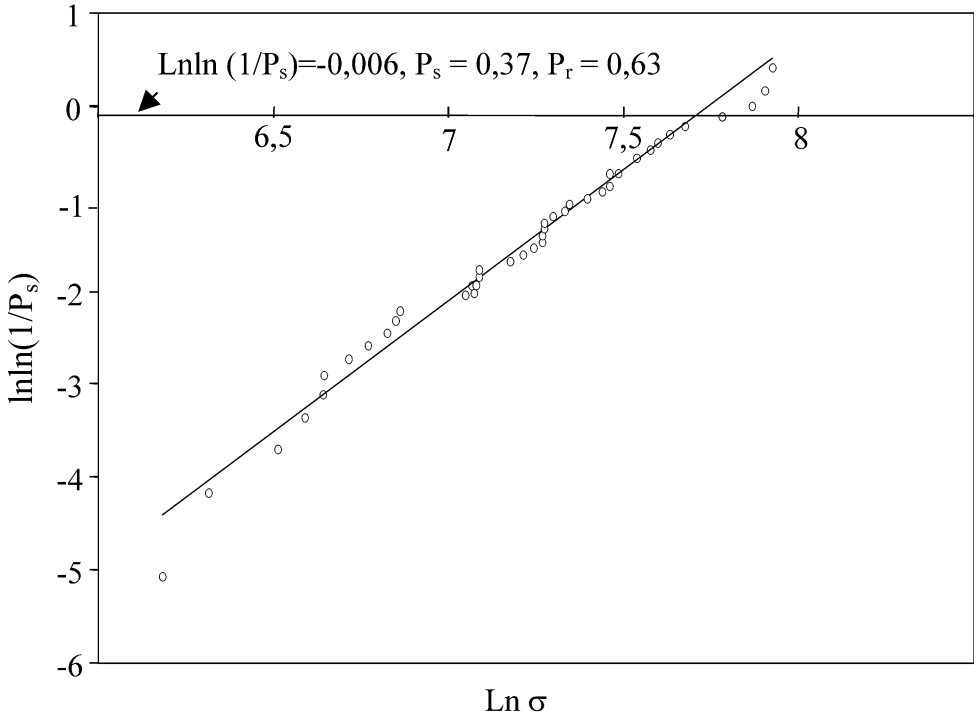

Fig. 2. Weibull plot of failure strengths of the fibres for a 10 mm gauge length.

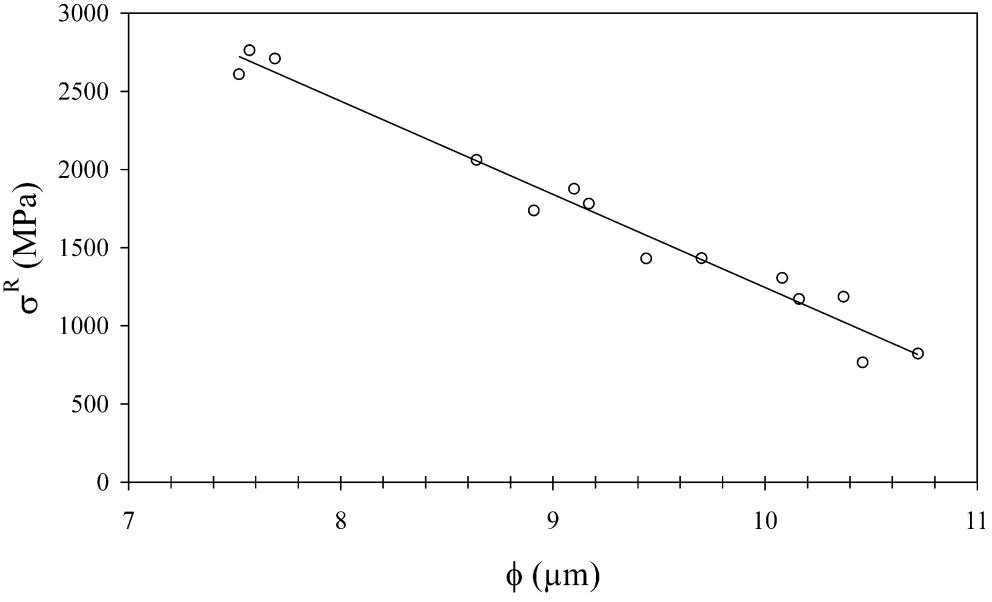

Fig. 3. Failure strength as a function of fibre diameter.

fibre and during the BN crystallization at high temperature.

3.3. Thermal decomposition of PolyMAB

The weight losses associated with polymer pyrolysis process are shown as a function of temperature (Fig. 6). Pyrolysis treatments are realized in a flow of NH_3/N_2 mixture in the temperature range from 25 to 1000 °C and in a flow of pure N_2 from 1000 to 1500 °C. Fig. 6 displays a typical TGA curve of the raw fibre and suggests that two important weight losses occur in the material as temperature is respectively increased, from T_g to 400 °C ($\Delta m = 20\%$) and from 400 to 1000 °C ($\Delta m = 23\%$). As shown in Table 3, when the raw fibre is heat treated up to 1000 °C, its chemical composition into carbon and hydrogen has decreased compared to the one of the polyMAB precursor (Table 1). The decrease into carbon and hydrogen composition is mainly due to the use of NH_3 as atmosphere gas up to

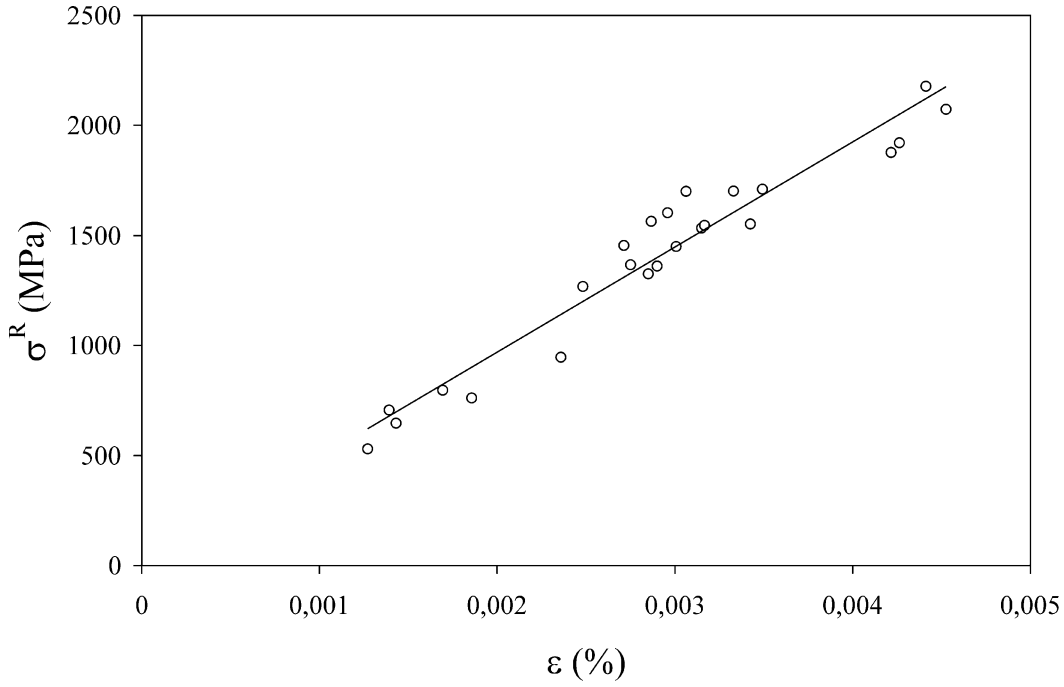

Fig. 4. Stress-elongation straight recorded for the fibre.

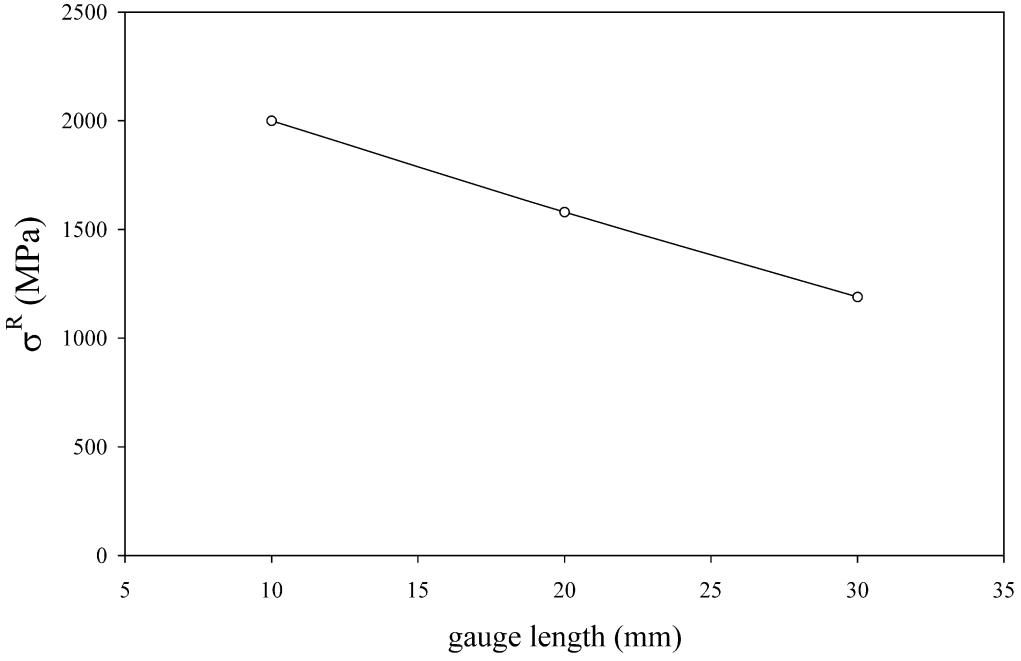

Fig. 5. Weibull plot of the failure strength for 10, 20 and 30 mm gauge lengths.

1000 °C. Indeed, during the thermal decomposition of polyMAB under pure N_2 atmosphere, the weight loss is less important due to the strong presence of carbon contaminant in the resulting material at 1000 and 1500 °C. The thermal decomposition is particularly low in a flow of N_2 up to the melt-spinning temperature compared with the thermal decomposition realized under NH_3 atmosphere in this temperature range. Such a low temperature polymer decomposition under pure NH_3 or NH_3/N_2 mixture atmosphere lead to cross-linking by carbon evolution from polyMAB. However, the polyMAB is not crosslinked under pure N_2 at low temperature and this is why the melt-spinning process is realized under N_2 atmosphere.

The high weight loss up to 1000 °C in a flow of NH_3/N_2 mixture evidences a considerable amount of gases evolved from polymeric fibre heated in the range 25–1000 °C that can explain the formation of defects in the

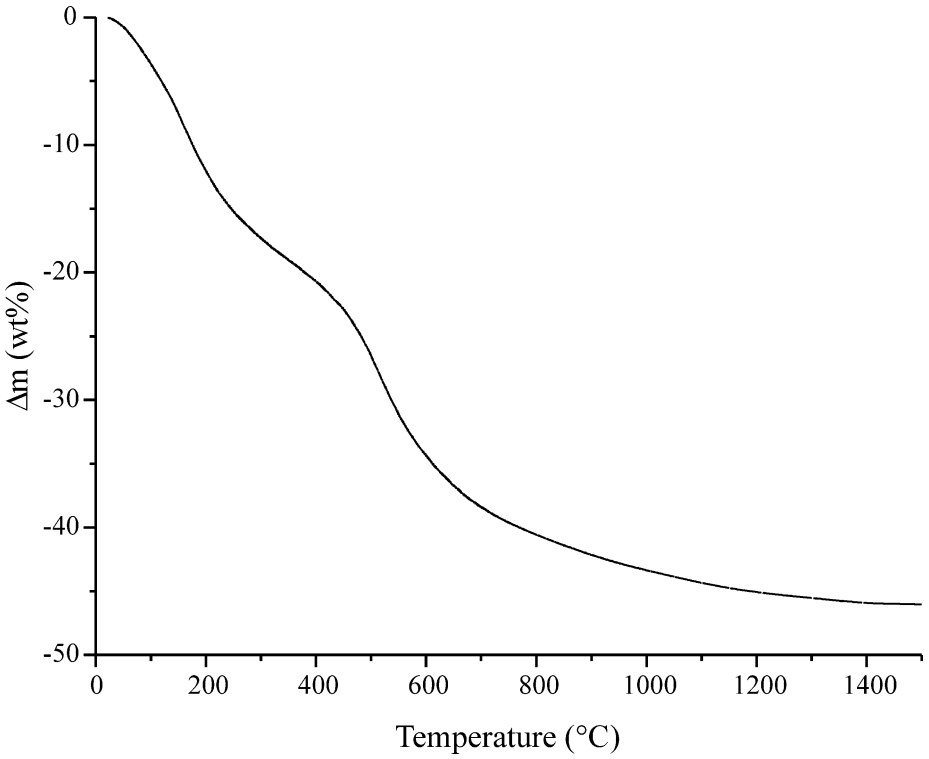

Fig. 6. TGA curve of the polymeric precursor.

Table 3
Elementary composition (wt.%) of mineral at 1000 °C

	C (wt.%)	H (wt.%)	N (wt.%)	B (wt.%)
Mineral 1000 °C	3.4	0.9	56.8	38.9

fibre volume. Above 1000 °C in pure N_2 atmosphere, the weight loss is low. The thermal decomposition is almost totally accomplished at 1400 °C and as can be seen, approximately 45 wt.% of the original polyMAB-based fibre is lost as a result of pyrolysis at 1500 °C. Conversely, the TGA curve indicates a BN yield from polyMAB of about 55% which is quite satisfactory with the used polymer.

3.4. Morphology of the BN fibre

Fig. 7. shows the general appearance of the high-performance fibre as seen with scanning electron microscopy (SEM). It is nearly circular (Fig. 7a) in cross section with a surface crenulated by shallow grooves (Fig. 7b). The cross section shows that the fibre consists of one homogeneous population of grains. The fibre exhibits a large amount of porosity on account of its granular texture due to the high temperature pyrolysis. Numerous mesopores and a few macropores are observed in the cross section (Fig. 7a). The micropores are not detectable but their presence can not be excluted. The definition of pore size follows the recommendations of IUPAC: micropore width less than 2 nm; mesopore width from 2 to 50 nm and macropore width greater than 50 nm. Sometimes, a few defects as cracks close to the surface (Fig. 7c) and fissures on the surface (Fig. 7d) are present when the fibre is pyrolyzed at high temperature. On their level, the texture is very stratified and a fragile point is created near the surface.

3.5. XRD analysis

Fig. 8 displays typical X-ray diffraction patterns in the 2θ range from 15 to 85° for the fibre before and after crushing. The peaks are characteristic of *h*-BN materials.[12] The XRD diffractogram of the fibre shows one intense peak corresponding to the (002) (2θ 26.8, $d = 0.334$ nm) reflection of *h*-BN. Two other peaks with very low intensity are observed and are indexed as the (10) ($41.6° < 2\theta < 43.9°$, 0.217 nm $< d < 0.206$ nm) and (004) ($2\theta 54.5°$, $d = 0.168$ nm) *h*-BN reflections. The resulting value of the interlayer distance d_{002} is reported in Table 4. The d_{002} spacing is close to theoritical value (0.333 nm) and pratically corresponds to the spacing of close-packed planes in a perfect *h*-BN crystal. The

Table 4
Textural parameters determined by means of XRD

	$I_{(002)}$ (%)	$I_{(10)}$ (%)	d_{002} (nm)	L_c (nm)	L_a(nm)	τ
Fibre	100	0.9	0.334	14	23	0.95
Crushed fibre	100	15				

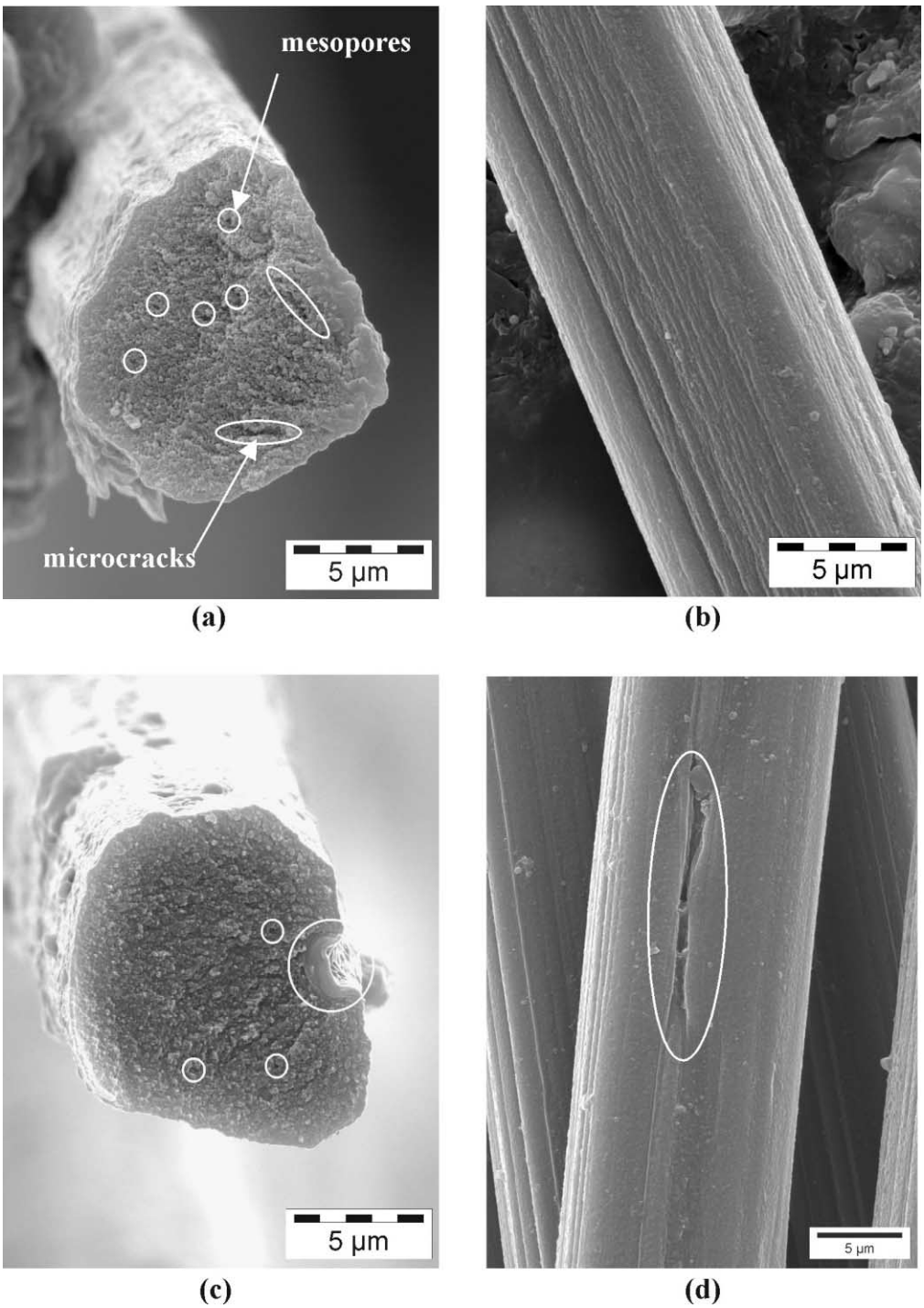

Fig. 7. SEM images of BN fibres: (a) cross-section; (b) longitudinal surface; (c) crack; (d) longitudinal fissure on the surface.

experimental peak of the (002) planes is relatively narrow showing a large crystallite size in the *c*-axis. The resulting values of the average crystallite sizes are summarized in Table 4. $\overline{L}_c$ measured is 14 nm. This value means that the average number of stacked layers in the crystallites is around 42. The accurate measurement of the $\overline{L}_a$ size is uncertain from the fibre pattern: generally, the intensity of the peak corresponding to the (10) planes is linked up to crystallite orientation along the a-axis and decreases when the order increases. This value is consequently determined by measuring the FWHM of the (10) peak on the crushed fibre pattern. The average BN crystal size $\overline{L}_a$ determined from the Scherrer relation is about 23 nm.

The XRD diffractogram of the fibre shows a pronounced preferred direction of (002) planes compared with the fibre-axis: the large ratio between (002) and (10) peak intensities evidences the orientation of crystallites

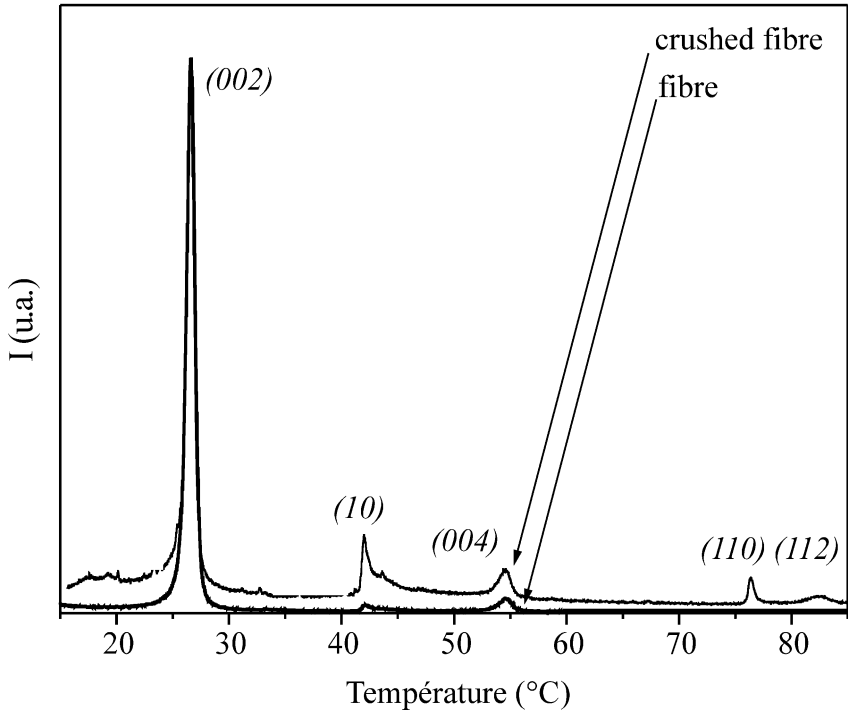

Fig. 8. Comparison of X-ray patterns of a BN fibre before and after crushing.

parallel to the fibre-axis. The degree of the preferred orientation of the (002) planes τ is about 0.95 (Table 4): on account of this high value, the (002) planes are pratically in fibre-axis. The fibre diffractogram presents some well-defined (hkl) diffraction lines. However, a number of characteristic lines reported for the hexagonal structure are missing: in particular the (102) diffraction line is not observed. This could not be considered conclusive evidence for the presence of a three-dimensional crystal structure.

3.6. TEM analysis

3.6.1. Longitudinal sections

Fig. 9 displays the SAD pattern performed on BN filaments from a longitudinal thin section. Electron diffraction has been found to be very effective in giving a semi-quantitative indication of the crystallite orientation degree compared with the fibre-axis. It has been used successfully to study the possible microstructural variation between the skin and core. In this high-performance BN fibre, the skin and core have the same structure and microtexture. Electron diffraction patterns with their (002), (10), (004) (110) and (112) arcs are typical of an anisotropic turbostratic material. The orientation of the hexagonal planes of BN compared with the fibre-axis is estimated from the spread angle along the (002) diffraction arc. The misorientation parameter ζ has an estimated value of 19° as shown in Table 5. The degree of alignment is 0.90: this value is similar to the one determined by XRD analysis. The

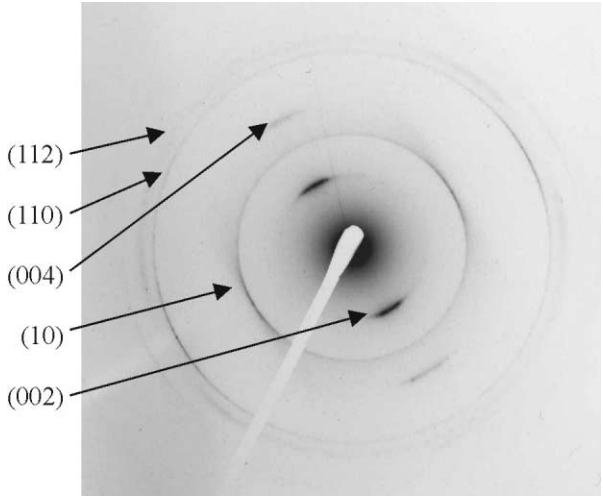

Fig. 9. SAD pattern of a BN fibre (longitudinal section).

Table 5
Textural parameters from TEM analysis

	ζ (°)	τ	L_c (nm)	L_a (nm)
Fibre BN	19	0.9	25	100

highly ordered structure of the fibre can explain why the fibre possesses high mechanical properties and, in particular, a high elastic modulus E (440 GPa). The bright-field (BF) and the (002) dark-field ((002) DF) images of similar regions of the h-BN fibre are reproduced in Figs. 10 and 11. This TEM investigation shows that the

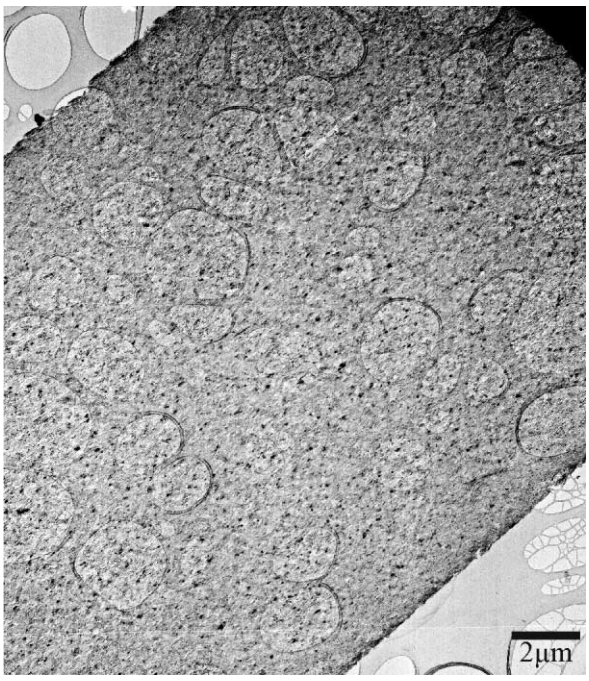

Fig. 10. Longitudinal section of a BN fibre.

high-performance BN fibre is homogeneous as the micrometric and nanometric scales (Fig. 10): the image obtained near the surface is the same from the one corresponding to the core of the fibre. As shown in Fig. 11, the bright-field image shows that the BN fibre has clearly a polycrystalline texture and the diffracting crystallites observed in (002) dark-field appear to consist of many smaller separate diffracting zones. It can be seen that the small luminous domains are pratically parallel to each other and to the fibre-axis indicating that the fibre has a high degree of orientation as calculating from the SAD pattern. The width and the length of the bright domains in the dark-field TEM image reflect the crystallite sizes: L_c and $L_{a//}$ can reach, respectively 25 and 100 nm. The dimensions are higher than the average ones calculated from X-ray diffraction data. On the other hand, the bright-field (BF) image evidences presence of mesopores and macropores between some crystallites in the longitudinal section.

The lattice-fringe image may directly reveal the way in which imperfections disturb the periodicity of a crystal. As it is shown in Fig. 12a, the (002) layers are pratically ordered and stacked parallel to the fibre-axis. The average number of stacked layers in the crystallites is about 80. It is also observed that a few crystallites are misoriented and not as well as organized parallel to each other and to the fibre-axis (Fig. 12b).

3.6.2. Transverse sections

The low magnification micrographs of transverse sections show a homogeneous texture (Fig. 13). As shown in Fig. 14, the dark crystallites in bright-field TEM image are not all diffracted and luminous in the dark-field images: some crystallites are relatively misoriented to each other. This random orientation is confirmed by the SAD pattern which is constituted of continuous rings (Fig. 15). The sizes of the bright domains in the dark-field micrograph reflects the crystal sizes (L_c, $L_{a\perp}$). They are close to the L_c, $L_{a//}$ values measured from the longitudinal section. The bright field (BF) image always

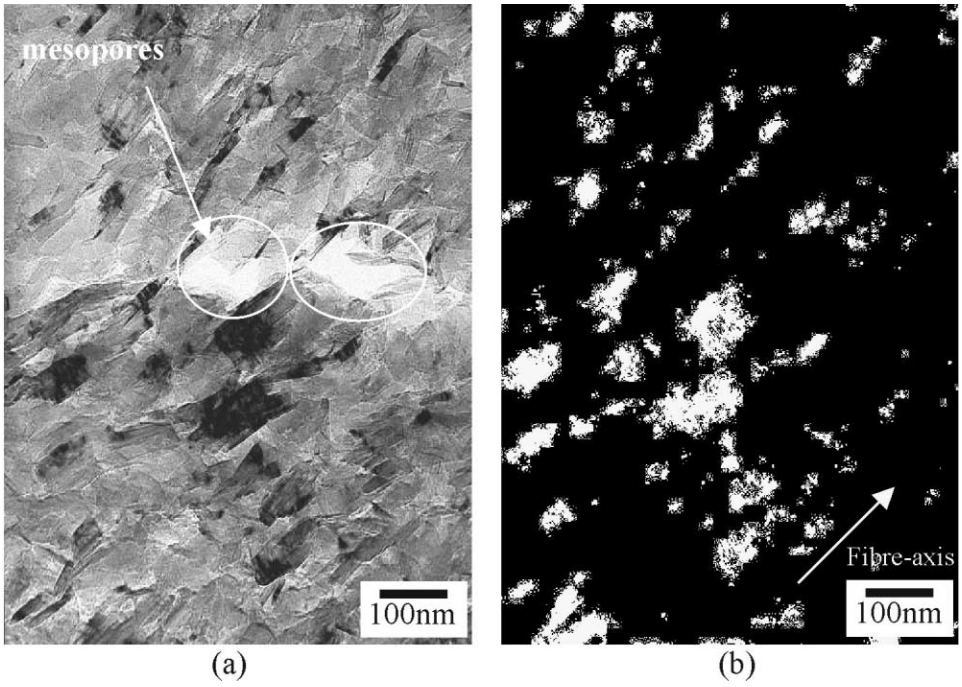

Fig. 11. TEM images of a BN fibre (longitudinal section): (a) BF image, (b) (002) DF image.

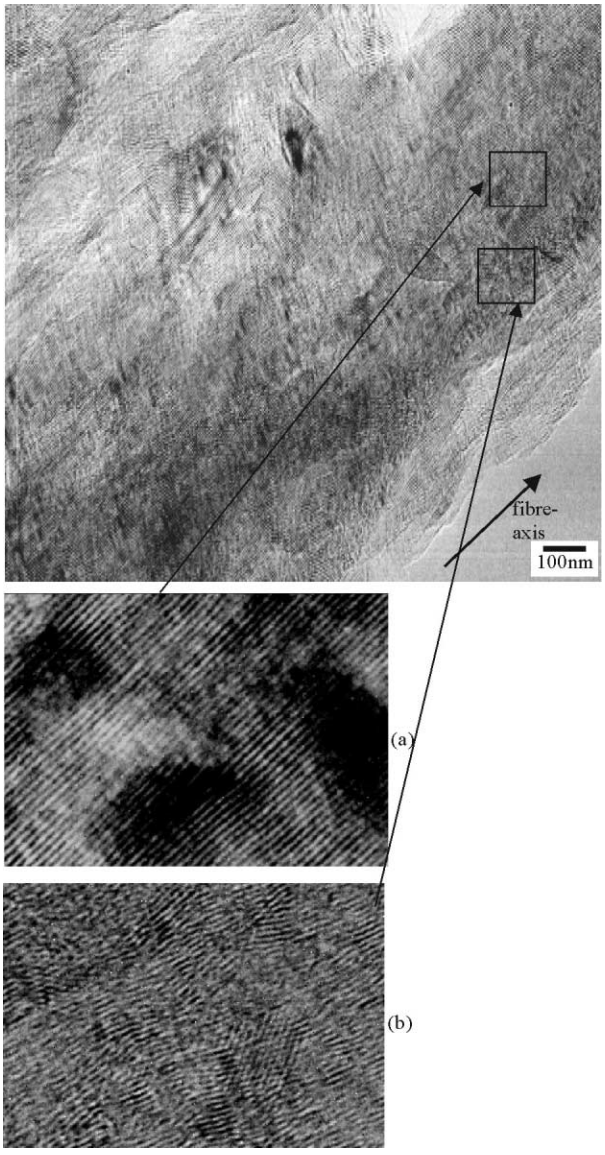

Fig. 12. Lattice fringes of a fibre (longitudinal section).

evidences some mesopore and macropore presence in the fibre.

4. Discussion

4.1. Defect and porosity-limited strength and density

The results of the mechanical tests clearly show an increase of the observed average tensile strength when the fibre gauge length decreases. Similarly, the observed average tensile strength increases when the diameter decreases. The dependence of the tensile strength with the volume of the fibre is a consequence of internal and surface defects evidenced by SEM. In this fibre, the internal and external defects rather appear with the increase of the pyrolysis temperature when a considerable

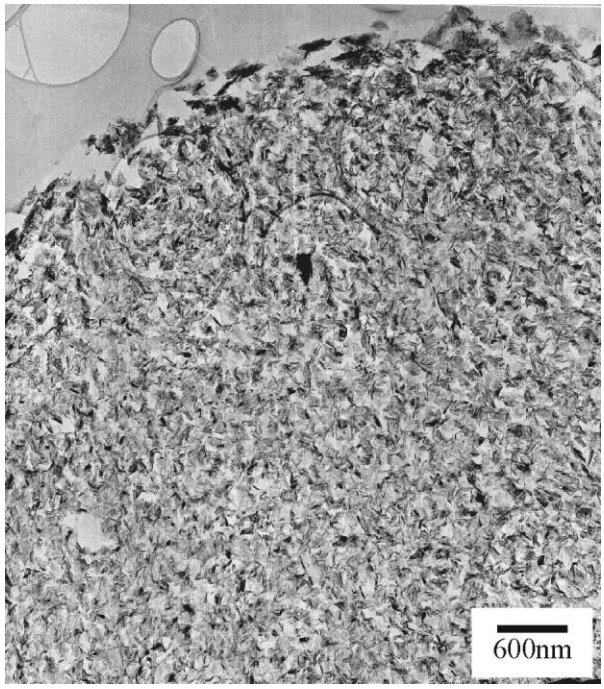

Fig. 13. Transverse section of the core and near the surface of a BN fibre.

amount of gaseous products is evolved from the polymeric fibre from 25 to 1000 °C. These gases formed during the pyrolysis can be responsible for gaseous inclusions as shown in Figs. 7, 11 and 14. The appearance of the internal flaws as mesopores and macropores can explain oneself by the slow diffusion of the gas throughout the solide phase which prevent their elimination during the transformation of organic structure in mineral structure from 400 to 1000 °C. These pores are still more numerous after the crystallization process when the granular microtexture expands in the fibre. The presence of the pores reduces the fibre density ($d=1.85$ g cm^{-3}). This value is very low compared to the theoritical density of the *h*-BN materials ($d=2.26$ g cm^{-3}) and Kimura's result ($d=2.05$ g cm^{-3}).[2] The porosity which represents 18% of the fibre volume limits the tensile strength ($\sigma^{R}=2000$ MPa). On the other hand, the large strength distribution is rather due to the surface defects. These surface defects as cracks are created during the crystallization process when the fibre is heated from 1300 to 1800 °C. The surface defects cause catastrophic breakings during the longitudinal tension applied to the fibre and they reduce the strength.

4.2. Effect of fibre microstructure upon the mechanical properties

The XRD pattern of the fibre shows a quasi-extinction of the (10) *h*-BN reflection. The (00l) *h*-BN reflections are always preponderating on account of preferential orientation of the crystallites in the fibre-axis. The

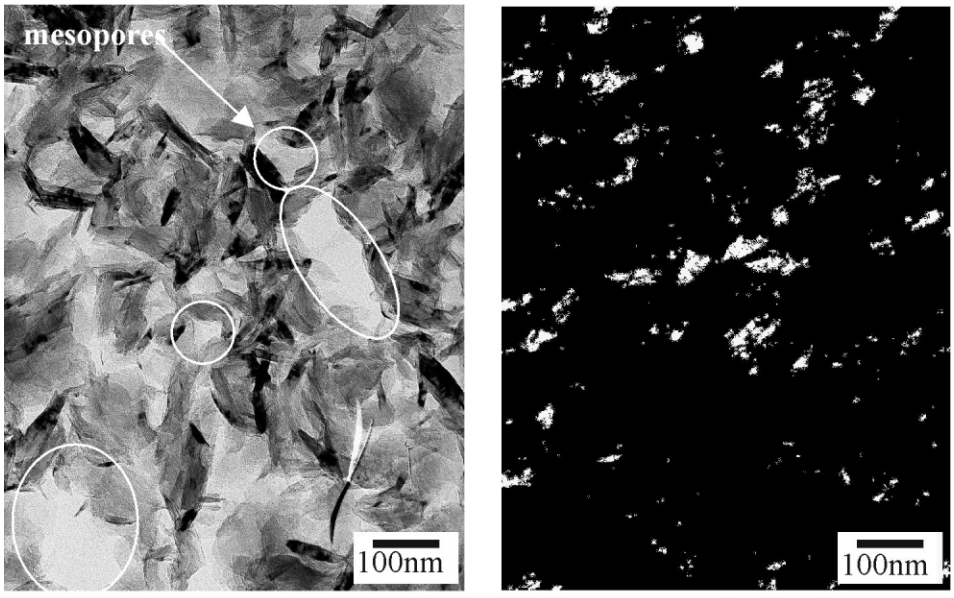

Fig. 14. Transverse section of a BN fibre: (a) BF image, (b) (002) DF image.

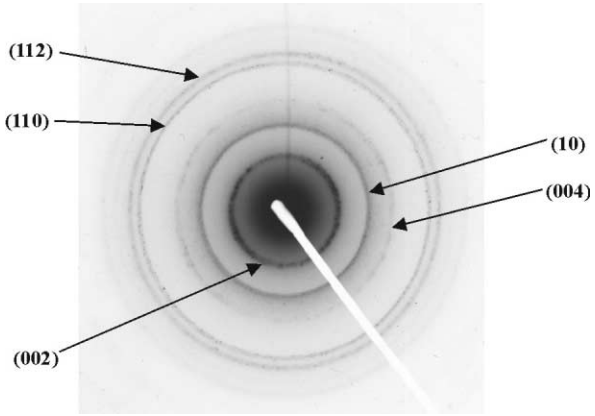

Fig. 15. SAD pattern of a BN fibre (transverse section).

accurate resolution of the broad peak (10) into the (100), (101) and (102) lines is not possible. The structure of the fibre consists of a turbostratic form with a minor phase of hexagonal structure in spite of the presence of the (112) peak. The interreticular distances (d_{002}, d_{004}) are very close to the theoretical values with 0.334 and 0.168 nm for the (002) and (004) planes against, respectively, 0.333 and 0.166 nm from well-crystallized *h*-BN materials. The longitudinal and transverse sections TEM images show that the fibre texture is constituted of crystallites with c-axis pratically perpendicular to fibre-axis. The SAD pattern is formed by short arcs for the (002) and (004) planes which evidence the good ordering of atomic planes whereas the other reflexions are characterized by a beginning of arcs or diffuse rings. The (002) arcs of electron diffraction patterns become closer to being spots, indicating high preferred orientation of the (002) planes in the fibre-axis.

The elastic modulus depends on the structural properties. It is known that interatomic bonds and basal plane stacking have an important effect on the mechanical properties. As a result, the theoritical tensile elastic modulus of the crystal in a direction parallel to the basal planes is very high. The planes are weakly bound and the properties are much lower in c-axis. As the theoritical modulus is high in the direction of *h*-BN basal planes, the mechanical properties of fibres could be determined by the degree of orientation of the *h*-BN basal planes in the fibre-axis. The high elastic modulus ($E = 440$ GPa) in fibre-axis is due to the high degree of crystallite orientation in the fibre-axis ($\tau = 0.90$). The high crystallite sizes calculated by TEM analysis ($L_c =$ 25 nm and $L_{a//} = L_{a//} > 80$ nm) pratically in the fibre-axis contribute to increase this high-modulus value. Moreover, the pyrolyze on the spool in our process can create stretching in the fibre volume which can increase the (002) planes alignment in the fibre-axis and, consequently, the longitudinal mechanical properties. The lower mechanical properties obtained by Kimura[2] are perhaps due to the absence of treatment with spool. Consequently, it is probable that the Kimura's pyrolysis was accomplished without stretching.

5. Conclusion

Mechanical properties of the BN fibre are essentially depending on their microtextural and structural properties. The polyMAB-based BN fibre presents a high modulus and a high strength in the fibre-axis with a high degree of layer plane orientation in the fibre-axis. The preferred orientation of the layer planes in the fibre-axis

and the elastic modulus are linked up whereas, in this high-performance fibre, the strength is rather depending on the presence of internal and external defects caused by the gases formed during the pyrolysis of polyMAB and the crystallization process. The internal defects as pores decrease the density of the fibre ($d = 1.85$ g cm^{-3}) which is low compared with the theoritical density.

References

1. Economy, J. and Anderson, R. V., Boron nitride fibers. *J. Polym. Sci*., 1967, **19**, 283–297.
2. Kimura, Y., Kubo, Y. and Hayashi, N., High-performance boron-nitride fibers from poly(borazine) preceramics. *Comp. Sci. Technol*., 1994, **51**, 173–179.
3. Paciorek, K. J. L. and Kratzer, R. H., Boron nitride preceramic polymer studies. *Eur. J. Solid State Inorg. Chem*., 1992, **29**, 101–112.
4. Narula, C. K., Schaeffer, R., Datye, A. and Paine, R. T., Synthesis of boron nitride ceramics from 2,4,6-triaminoborazine. *Inorg. Chem*., 1989, **28**, 4053–4055.
5. Wideman, T., Remsen, E. E., Cortez, E., Chlanda, V. L. and Sneddon, L. G., Amine-modified polyborazylenes: second-generation precursors to boron nitride. *Chem. Mater*., 1998, **10**, 412–421.
6. Bernard, S., Bonnetot, B., Cornu, D., Favre, R., Miele, P., Toury, B., Toutois, P. and Vincent, H. Fibres BN de haute performance et leur procédé d'élaboration. French Patent 0003380, 16 March 2000.
7. Bernard, S., Berthet, M.P., Bouix, J., Cornu, D., Miele, P., Toury, B., Toutois, P. & Vincent, C., Procédé de fabrication de fibres de nitrure de bore à partir d'aminoborazines, French Patent 0003377, 16 March 2000.
8. Patankar, S. N., Weibull distribution as applied to ceramic fibres. *J. Mater. Sci. Let*., 1991, **10**, 1176–1181.
9. Mignani, G., Richard, C. and Trichon, R., Procédé de préparation de polyaminoborazines, French patent 2695645, 15 September 1992.
10. Nemanich, R. J., Solin, S. A. and Martin, R. M., Light scattering study of boron nitride microcrystals. *Phys. Rev. B*, 1981, **23**, 6348–6356.
11. Miller, F. A. and Wilkins, C. H., Infrared spectra and characteristic frequencies of inorganic ions. *Anal. Chem*., 1952, **24**, 1253–1294.
12. Thomas, J., Weston, N. E. and O'Connor, T. E., Physical and inorganic chemistry. *Am. Chem. Soc*., 1963, **84**, 4619–4622.